

Role of social interactions in dynamic patterns of resource patches and forager aggregation

Nessy Tania^a, Ben Vanderlei^b, Joel P. Heath^c, and Leah Edelstein-Keshet^{c,1}

^aDepartment of Mathematics and Statistics, Smith College, Northampton, MA 01063; ^bDepartment of Mathematics and Statistics, University of the Fraser Valley, Abbotsford, BC, Canada V2S 7M8; and ^cDepartment of Mathematics, University of British Columbia, Vancouver, BC, Canada V6T 1Z2

Edited by Mark A. Lewis, University of Alberta, Edmonton, Canada, and accepted by the Editorial Board June 4, 2012 (received for review January 31, 2012)

The dynamics of resource patches and species that exploit such patches are of interest to ecologists, conservation biologists, modelers, and mathematicians. Here we consider how social interactions can create unique, evolving patterns in space and time. Whereas simple prey taxis (with consumable prey) promotes spatial uniform distributions, here we show that taxis in producer–scrounger groups can lead to pattern formation. We consider two types of foragers: those that search directly (“producers”) and those that exploit other foragers to find food (“scroungers” or exploiters). We show that such groups can sustain fluctuating spatiotemporal patterns, akin to “waves of pursuit.” Investigating the relative benefits to the individuals, we observed conditions under which either strategy leads to enhanced success, defined as net food consumption. Foragers that search for food directly have an advantage when food patches are localized. Those that seek aggregations of group mates do better when their ability to track group mates exceeds the foragers’ food-sensing acuity. When behavioral switching or reproductive success of the strategies is included, the relative abundance of foragers and exploiters is dynamic over time, in contrast with classic models that predict stable frequencies. Our work shows the importance of considering two-way interaction—i.e., how food distribution both influences and is influenced by social foraging and aggregation of predators.

pattern formation | foraging strategies | ecological patchiness | chemotaxis | spatial ecology

In this paper, we study the dynamics of social interactions to explore the consequences for spatiotemporal population structure and dynamics. We show that interactions among individuals are key for pattern formation and self-organization when foragers either follow gradients of food or socialize with those that do. Our aim is to demonstrate that social interactions among foragers could have particularly important implications for spatial models of forager–resource dynamics. A comprehensive understanding of the spatial dynamics of social foraging needs to consider the two-way dynamic interaction between forager aggregation and resource patchiness, a problem that remains poorly understood (1, 2).

A secondary theme is the discovery of another pattern-forming mechanism. Nature abounds with patterns that the human eye is adept at picking out. Patterns occur in chemical, physical, and biological systems on many scales, from distribution of proteins in a cell, and tissue morphogenesis, to patchy distribution of species in ecology (3–5, 6). There is great interest in finding both universal mechanisms for such patterns (e.g., the balance of repulsion–attraction forces, local activation and long-range inhibition, or motion in an external field; ref. 7), as well as specific examples that have rich pattern-forming features (8).

Patterns formed by organisms, and the way they shape their environment, is a rich area with physical (phase transitions), engineering (robotics), sociological (e.g., human traffic patterns), and ecological implications (5, 9–11). Social foraging in mixed-species groups and the emergent patterns of distributions have been studied in ecology (e.g., ref. 12). Rules of individual behavior in socially cohesive foraging and/or migrating groups have

been explored recently in empirical and theoretical studies (13, 14).

In studying social foraging, our goal was to use a spatially explicit analytical framework. There is great interest in extending analytical and empirical studies to understanding the spatiotemporal dynamics of social aggregation, although tools for doing so are as yet emerging. Both individual-based models tracking single organisms (14) and density-based theories using partial differential equations (PDEs) (8, 17) contribute to such technology. The Keller–Segel (KS) model (18) provides a great avenue for exploration that already has a history to build on. This model is classical, based on a continuum approximation, and depicts a mechanism for spatial aggregation. Although explored in vast literature, KS has yet to be applied to the situation of dual social behavior here described, but see the individual-based model for gradient climbers and their highly social followers (14). Further, how organisms shape and are in turn affected by the spatial distribution of their resources is still an emerging area of research, addressed in this paper.

In group foraging studies, resource distribution, patch size and structure, and distance between foragers were shown to influence the “finders’ share” (food obtained by producers vs. scroungers) (1, 15, 16), which motivated us to ask which strategy confers an advantage under various conditions. To do so, we ask how limited resource distribution, patch size, and movement/search parameters contribute to relative success, quantified by a ratio of net food consumed by foragers vs. exploiters. Recent spatially explicit simulations to explore this question were based on simulations of agent-based producer–scrounger models (1). Such studies suggest that social interactions should increase with decreasing patch encounter rate. These recent findings emphasize the need for spatially explicit approaches in social foraging theory.

We conclude by investigating how switching between strategies (within a generation) affects the relative abundance of each behavioral type. We also consider a similar question on the time-scale of many generations, when success of each strategy determines reproductive fitness.

Taxis Models

To understand spatial aggregation patterns, modelers often formulate simple models that can be investigated analytically or computationally. Some models track single individuals, positing rules of interaction (1, 9) and others formulate equations to describe densities of populations. Most such models are PDEs (17) or (if nonlocal) integro-PDEs (20).

Author contributions: J.P.H. provided initial concept; N.T. performed analysis; N.T., B.V., J.P.H., and L.E.-K. designed research; N.T., B.V., J.P.H., and L.E.-K. performed research; and N.T., B.V., J.P.H., and L.E.-K. wrote the paper.

The authors declare no conflict of interest.

This article is a PNAS Direct Submission. M.A.L. is a guest editor invited by the Editorial Board.

¹To whom correspondence should be addressed. E-mail: keshet@math.ubc.ca.

This article contains supporting information online at www.pnas.org/lookup/suppl/doi:10.1073/pnas.1201739109/-DCSupplemental.

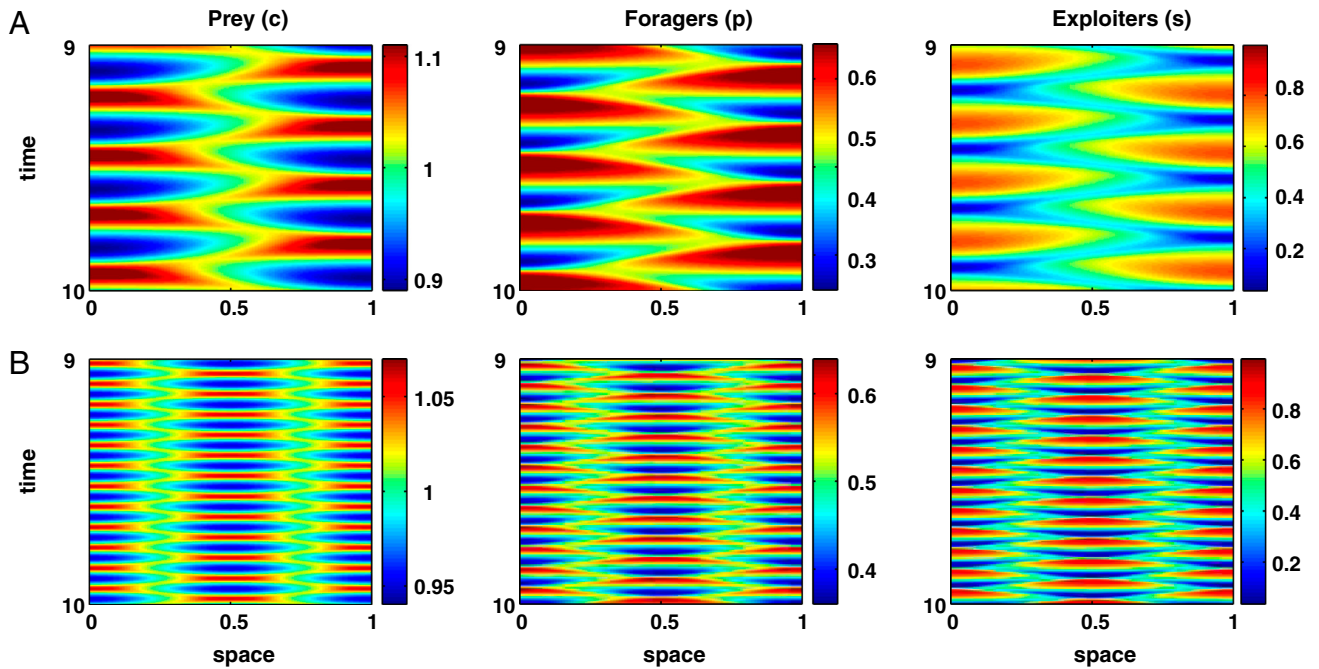


Fig. 2. Oscillatory spatial patterns in prey, forager, and exploiter densities for two values of exploiter taxis parameter v_s . Horizontal axis is space; vertical axis is time. Exploiter taxis parameter: (A) $v_s = 10$ and (B) $v_s = 20$. Other parameter values were $v_p = 10$, $\mu = 0.05$, $\lambda = 8.0$, $r = 8.05$, and $d = 0.1$.

ager groups (low v_s), instability is less likely, all else being equal. If v_s is large enough, inequality [3] implies that (i) increasing the mobility (through d) or decay rate of prey (through μ or the predation rate λ) is stabilizing, whereas (ii) increasing the prey–taxis coefficient (v_p) is destabilizing. Finally, (iii) the fraction of foragers (ϕ_p) also plays a role. We plot the left-hand side of [3] vs. ϕ_p in Fig. 1. Satisfying the inequality restricts ϕ_s to an intermediate range. For example, for $v_s = 10$ and $v_p = 10$, instability occurs for $0.14 \leq \phi_p \leq 0.64$.

We find that instability and spatial patterning is accompanied by temporal oscillations. (In the *SI Appendix*, we show that this instability stems from a Hopf bifurcation.) Linear stability analysis also predicts that, at some lower value of v_s , a single mode becomes unstable, whereas higher v_s allows for a range of unstable modes.

To visualize the resulting spatiotemporal dynamics, we carried out simulations of the system [2]. Fig. 2 shows the results for two values of v_s (Movies S1–S2). Starting from a nearly uniform distribution of foragers, exploiters, and resource, we observed growth of periodic waves. By $t = 9$, these fluctuations settle into regular cycles. For a smaller value of v_s (Fig. 2, Upper), a single “hot spot” (red) alternates between one and the other end of the domain. We can understand this behavior by noting that local aggregations of animals deplete the food, which takes time to renew. Meanwhile, movement toward undepleted food resources sets up growing fluctuations. It is these waves of pursuit that lead to the observed periodic fluctuation in the densities of the variables.

If the parameter v_s is increased (Fig. 2, Lower), the frequency of oscillation increases and a larger numbers of hot spots occur (resulting from instability of higher modes) with concurrent decrease in amplitudes of p and c . In the limit of high v_s , the system reduces back to the simple forager–resource system that has no spatial instability: This is the case in which the exploiters track foragers so efficiently that the motion of the two groups is practically indistinguishable. In this limit, the pattern can no longer be sustained, and only the spatially uniform state is stable.

So far, analysis and simulations were confined to 1D. We asked what the model predicts in higher dimension. This question is of interest because it is well-known that KS chemotactic equations

can develop singularities and “blowup” solutions in finite time in 2D and 3D (21). We repeated this computation in 2D. As shown in the *SI Appendix* and Movies S3–S8, the oscillatory patterns of aggregation are also evident in the 2D setting. In contrast to the positive feedback in the KS model, here prey depletion serves as a negative feedback, preventing sharp peaks/singularities (due to aggregation) from occurring.

Advantages of the Strategies: Foraging Versus Exploiting

To compare the two strategies, we reasoned that at any given time, an individual of a given type has an opportunity to feed proportional to its per-capita contact with food—i.e., $c(x, t)p(x, t)/\phi_p$ or $c(x, t)s(x, t)/\phi_s$. We defined $F_p(t)$, $F_s(t)$ as the cumulative per-capita food intake for foragers and exploiters, respectively (obtained by integrating the contact rates over the domain, up to time t ; see *SI Appendix* for details). Then the ratio $B(t) = F_s/F_p$ can be used to compare the relative advantage of the strategies. We also denote $b(t)$ as the ratio of instantaneous per-capita food intake—i.e., without integration over time. $B = 1$ implies both strategies are equally successful, whereas $B > 1$ corresponds to an advantage for exploiters. We consider both static and dynamic versions of this measure.

Relative Advantages for a Static Food Patch

We first considered a static spatially nonuniform food distribution $c(x)$ with analytically solvable steady-state forager/exploiter profiles $p(x)$, $s(x)$ and time-independent relative-advantage B . We chose a unimodal food distribution $c(x) = \cos(\pi x) + 1$ to satisfy no-flux boundary conditions for p and s . In Fig. 3, we numerically generated the curve of neutral advantage $B = 1$ in the v_p – v_s plane for various values of the forager fraction ϕ_p (see *SI Appendix*). Exploiters do best when (v_p, v_s) is above the curve vs. foragers below the curve. At a fixed forager acuity v_p , exploiters with v_s above some threshold have greater advantage. Foragers with low v_p are weakly attracted to food, so their density forms shallow gradients; then only exploiters with high acuity would detect such slight forager density gradients. For larger v_p , the foragers concentrate at food sources, forming sharper density gradients, so the threshold v_s value is lower. Larger ϕ_p shifts the $B = 1$ curve

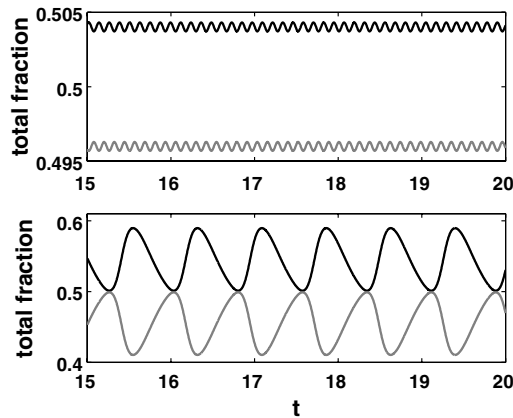


Fig. 6. The fractions of foragers and exploiters over time in the case of strategy switching. Parameter values as in Fig. 2, but with $v_p = 10$, $v_s = 10$, $k = 4$ (Upper), and $v_p = 1$, $v_s = 20$, $k = 19$ (Lower). Black curves indicate the fractions of foragers and gray curves for the fractions of exploiters.

the uniform steady state is $\phi_s = \phi_p$. Simulation results are shown in Fig. 6. For parameter values in Fig. 2, switching leads to hardly perceptible oscillations of strategies close to $p \approx s \approx 0.5$ (Fig. 6, Upper). Other parameter values, however, accentuate the cycles (Fig. 6, Lower; spatial patterns shown in *SI Appendix*, Fig. S7, and *Movie S9*). Such results reinforce the idea that spatial interactions can lead to behavioral transitions as well as dynamic forager-exploiter distributions. In contrast to a classic result where social interactions led to a fixed frequency of forager and exploiter (22), we observed temporal variations in the frequencies.

Further exploring the full spatiotemporal model, we found that switching can both promote or suppress instability, by shifting the critical v_s value at which oscillatory pattern emerges. Switching at constant rates, for example, yields new spatiotemporal patterns, not seen otherwise, including standing wave patterns (see *SI Appendix*, Fig. S6).

Next, we considered how reproductive fitness could affect the population structure over several generations. To do so, we omitted the short-term behavioral switching ($h_s = h_p = 0$), and assumed, instead, the semelparous reproduction rule

$$s(T + 1) = F_s(T)/F(T), \quad p(T + 1) = F_p(T)/F(T), \quad [5]$$

for T the generation number, and $F = F_s + F_p$. Now [2] captures within-generation dynamics, whereas [5] relates reproductive fitness between generations to the relative success within a genera-

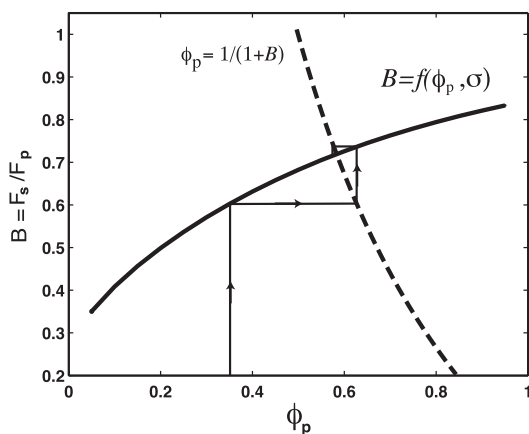


Fig. 7. When relative advantage of strategies affects the proportions of foragers and exploiters in the next generation (dotted curve), the fraction ϕ_p changes, here approaching a steady state. Solid curve: $f(\phi_p, \sigma)$, $\sigma = 0.05$ from Fig. 4.

tion (while keeping population size fixed). Other cases with net population growth can be simulated by alternating the model of [2] (within a generation) with arbitrary fitness-based reproduction rule (see *SI Appendix*).

Rewritten, [5] yields $\phi_p(T + 1) = 1/[1 + B(T)]$ (dotted curve in Fig. 7). At each generation T , given $\phi_p(T)$, we can compute $B(T)$ by integrating food consumed by each strategy over the forager's lifespan. One such curve, $B(T) = F_s/F_p = f(\phi_p(T), \sigma)$ for σ -sized food patch shown in Fig. 4 is copied on Fig. 7 ($\sigma = 0.05$). Together, such two rules link intergenerational values of ϕ_p and B . A cobweb diagram based on this proof of principle illustrates convergence of ϕ_p to a unique stable equilibrium over several generations. Stable cycles are also possible, as discussed in the *SI Appendix*, Fig. S10, provided the function $f(\phi_p(T), \sigma)$ is steep enough. Thus, a variety of long-term dynamics are possible, and provide future directions to explore, based on various assumptions about the food, the fitness measure, and dynamics between and within generations.

Discussion

Social foraging models (2, 23) have addressed interactions in the context of information sharing (24) and frequency dependent dynamics (22, 25). One subset of such models examines so-called producer–scrounger systems wherein one species (the scrounger) exploits another (the producer). Most such investigations fail to account for spatially explicit interactions (16, 22, 25), which have been the focus of our paper.

Our results have two major thrusts. First, in a context of pattern formation, we revisited the classic prey–taxis model and showed that inclusion of exploiters leads to spontaneously emergent patterns (absent in the original model). Such results apply to a class of ecological models that fall under the rubric of producer–scrounger systems, although these have not been extensively studied in the literature. (One notable exception is Beauchamp, ref. 1, who indicated that spatial producer–scrounger systems could be self-organizing.) Using analytic techniques such as LSA, we found conditions on the parameters [3] for such patterns to occur, finding persistent spatiotemporal oscillations stemming from a Hopf bifurcation. These patterns form a stable attractor of the dynamics in both 1D (Fig. 2, *Movies S1–S2*) and 2D (*Movies S3–S8*). Heuristically, the primary foragers detect weak resource gradients, congregate, and form detectable “crowd gradients” to which exploiters respond. These interactions result in an inherent delay: It takes time for forager gradients to form in response to the prey distribution, and the exploiters can react only once such gradients are noticeable. This lag leads to waves of pursuit that arise spontaneously, with concomitant patchiness in the resource distribution.

In ecology, a common basic assumption is that resources are patchily distributed (26, 27) and that this influences competitive advantage of various strategies (28). Recent studies suggest that the amount of food obtained by producers vs. scroungers (the finders' share), can depend strongly on patch structure and distances between individuals (1, 15, 16). This idea motivated our second major thrust, to explore the relative benefits of the two social foraging strategies in the model. We quantified benefit in terms of resources available to each strategy. In the case of fixed strategies and static resource distribution, we found (using convenient closed-form solutions of the system) how relative success depends on the relative acuity and abundance of each species (taxis parameters v_s , v_p and forager fraction ϕ_p). For a fixed forager taxis parameter v_p , exploiters do better as v_s increases, or as the fraction of foragers ϕ_p (and hence the steepness of their gradient) increases. Exploiters also “win” at fixed intermediate values of v_s and small ϕ_p for large v_p , again due to sharp gradients of foragers they can detect. Both ideas relate to ways of crossing the neutral curve $B = 1$ shown in Fig. 3. In the case of exhaustible food patches, the strategies are equal only when resources are

The role of social interactions in dynamic patterns of
resource patches and forager aggregations
Supplementary Information Appendix

Nessy Tania ¹, Ben Vanderlei ², Joel Heath ³, and
Leah Edelstein-Keshet ³

¹ Department of Mathematics and Statistics, Smith College,
Northampton, MA 01063

² Department of Mathematics and Statistics, University of the Fraser Valley,
Abbotsford, BC V2S 7M8, Canada

³ Department of Mathematics, University of British Columbia,
Vancouver, BC V6T 1Z2, Canada

10.1073/pnas.1201739109

Contents

1	Simple Forager Model	2
1.1	Nondimensionalization	2
1.2	Linear Stability Analysis of the Uniform Steady State	3
2	Foragers and Exploiters Model	5
2.1	Nondimensionalization	5
3	Advantage of Strategies for Exploiters vs Foragers	6
3.1	Relative advantages with a static food patch	6
3.2	Relative advantage with a nonrenewable resource.	7
3.3	Model variants	8
4	Linear Stability Analysis for Foragers-Exploiters Model	10
5	Switching between the strategies	14
5.1	Random switching	14
5.2	Switching based on perceived relative advantage	14
5.2.1	Purely local sensing	15
5.2.2	Long range (global) sensing	16
5.2.3	Finite sensing range	16
6	Reproductive fitness depends on relative advantage of strategies	17
7	Numerical Methods	20

1 Simple Forager Model

We start by considering a simplified model in which only the interactions between foragers and food are tracked. Let $P(x, t)$ be the density of the predator/forager, and $C(x, t)$ density of prey/food. We assume that foragers and prey items have some random motion (motility coefficients D_p and D_c respectively), and that foragers are attracted by the gradient of prey with taxis coefficient χ_p . Upon encounter by foragers, prey is consumed at a rate Λ . Finally, prey accumulates (by migration or reproduction at rate R) and decays (rate M). We consider motion within a one-dimensional domain of length L . The equations are

$$\frac{\partial P}{\partial t} = D_p \frac{\partial^2 P}{\partial x^2} - \chi_p \frac{\partial}{\partial x} \left(P \frac{\partial C}{\partial x} \right), \quad (\text{S1a})$$

$$\frac{\partial C}{\partial t} = D_c \frac{\partial^2 C}{\partial x^2} - \Lambda P C - M C + R. \quad (\text{S1b})$$

We assume that movements of forager and prey are constrained to be within the domain by imposing no-flux boundary conditions,

$$\left. \frac{\partial P}{\partial x} \right|_{x=0,L} = 0 \quad \text{and} \quad \left. \frac{\partial C}{\partial x} \right|_{x=0,L} = 0. \quad (\text{S2})$$

This guarantees that the total forager population remains constant,

$$\int_0^L P(x, t) dx = \Phi_p. \quad (\text{S3})$$

The system above has a spatially-uniform steady state solution,

$$P(x, t) = \frac{\Phi_p}{L} \quad \text{and} \quad C(x, t) = \frac{R}{\Lambda(\Phi_p/L) + M}. \quad (\text{S4})$$

1.1 Nondimensionalization

To minimize the number of parameters in the following analysis, we first nondimensionalize the model as follows:

$$x = \hat{X} \bar{x}, \quad t = \hat{T} \bar{t}, \quad P = \hat{P} \bar{p}, \quad C = \hat{C} \bar{c}, \quad (\text{S5})$$

where $\hat{X}, \hat{T}, \hat{P}, \hat{C}$ are the scaling constants, and $\bar{x}, \bar{t}, \bar{p}, \bar{c}$ are the non-dimensional variables. We then choose the following nondimensionalization/scaling constants:

- The space variable x is scaled by the length of the domain, $\hat{X} = L$. Note that, \bar{x} then ranges from 0 to 1.
- Time t is scaled by the timescale of a random search by foragers over distance L , $\hat{T} = L^2/D_p$.
- The forager density P is scaled by the average density over the domain, $\hat{P} = \Phi_p/L$.

- The food density C is scaled by the maximum level of the initial food density, $\hat{C} = C_{max} = \max_{0 \leq x \leq L} C(x, 0)$.

This results in the following set of non-dimensionalized equations:

$$\frac{\partial \bar{p}}{\partial \bar{t}} = \frac{\partial^2 \bar{p}}{\partial \bar{x}^2} - v_p \frac{\partial}{\partial \bar{x}} \left(\bar{p} \frac{\partial \bar{c}}{\partial \bar{x}} \right), \quad (\text{S6})$$

$$\frac{\partial \bar{c}}{\partial \bar{t}} = d \frac{\partial^2 \bar{c}}{\partial \bar{x}^2} - \lambda \bar{p} \bar{c} - \mu \bar{c} + r. \quad (\text{S7})$$

The new dimensionless parameters are:

- $v_p = \frac{\chi_p \hat{C} \hat{T}}{L^2} = \frac{\chi_p C_{max}}{D_p}$. Thus, if there is an increase by one \hat{C} unit of food density over distance L , the forager will move with speed $v_p D_p / L$. Additionally, we can also interpret v_p as the ratio of the timescale for random walk to that for taxis (over one unit of food gradient):

$$v_p = \frac{\text{random walk timescale}}{\text{taxis timescale}} = \frac{L^2 / D_p}{L / (\chi_p \hat{C} / L)} \quad (\text{S8})$$

- $d = D_c / D_p$ defines the ratio of mobility of prey compared to predators.
- $\lambda = \Lambda \hat{T} \hat{P} = \frac{\Lambda L \Phi_p}{D_p}$ i.e. λ / \hat{T} is the typical rate of prey consumption by a typical predator population size Φ_P .
- $\mu = M \hat{T} = \frac{M L^2}{D_p}$ and $r = R \hat{T} / \hat{C} = \frac{R L^2}{D_p C_{max}}$, similarly, are the non-dimensional rates of prey death/emigration and birth/immigration respectively.

The conservation of predators (S3) becomes $\int_0^1 \bar{p}(\bar{x}, \bar{t}) d\bar{x} = 1$. For the remainder of this section, we drop the bar superscript from all the non-dimensionalized variables.

1.2 Linear Stability Analysis of the Uniform Steady State

We consider

$$\frac{\partial p}{\partial t} = \frac{\partial^2 p}{\partial x^2} - v_p \frac{\partial}{\partial x} \left(p \frac{\partial c}{\partial x} \right), \quad (\text{S9a})$$

$$\frac{\partial c}{\partial t} = d \frac{\partial^2 c}{\partial x^2} + h(c, p), \quad (\text{S9b})$$

For generality, we leave $h(c, p)$, as an unspecified function with only the following restrictions:

- $h_p = \frac{\partial h}{\partial p} < 0$ reflecting prey consumptions by foragers.

- $h_c = \left. \frac{\partial h}{\partial c} \right|_{(c=c_0, p=p_0)} < 0$, where $h(c_0, p_0) = 0$.

The second condition guarantees that the corresponding spatially uniform (ODE) system has a stable steady state solution. As p is conserved, in the spatially uniform case, it remains as a constant parameter, specifically, $p = p_0 = 1$ as determined by the conservation equation. The corresponding ODE consists of a single equation $\frac{dc}{dt} = h(c, p_0)$, and (c_0, p_0) is a stable equilibrium of that ODE.

Note that the result to be presented below is independent of the functional form of $h(c, p)$ as long as this stability condition is satisfied. For example, we can assume a linear prey death and constant renewal rate, $h(c, p) = -\lambda pc - \mu c + r$, or incorporate a logistic growth of prey, $h(c, p) = -\lambda pc + rp \left(1 - \frac{p}{K}\right)$.

The spatially uniform steady state solution, of the PDEs corresponds to $p(x, t) = p_0 = 1$ and $c(x, t) = c_0$ (obtained by setting $h(c_0, p_0) = 0$). To analyze the stability of the uniform steady-state solution, we introduce *small* perturbation $\tilde{p}(x, t)$ and $\tilde{c}(x, t)$ about the uniform solution, i.e. consider

$$p(x, t) = p_0 + \tilde{p}(x, t) \quad \text{and} \quad c(x, t) = c_0 + \tilde{c}(x, t). \quad (\text{S10})$$

Substituting these back into (S9) and linearizing about (p_0, c_0) , we obtain

$$\frac{\partial \tilde{p}}{\partial t} = \frac{\partial^2 \tilde{p}}{\partial x^2} - v_p p_0 \frac{\partial^2 \tilde{c}}{\partial x^2}, \quad (\text{S11a})$$

$$\frac{\partial \tilde{c}}{\partial t} = d \frac{\partial^2 \tilde{c}}{\partial x^2} + h_p \tilde{p} + h_c \tilde{c}, \quad (\text{S11b})$$

where h_p, h_c are partial derivatives of $h(c, p)$ evaluated at (c_0, p_0) . With the no-flux boundary conditions, the linearized system can be solved by looking for solution of the form,

$$\tilde{p}(x, t) = p_1 \cos(qx) e^{\omega t} \quad \text{and} \quad \tilde{c}(x, t) = c_1 \cos(qx) e^{\omega t}. \quad (\text{S12})$$

with $q = \pm\pi, \pm 2\pi, \dots$. Substituting back into (S11), we obtain the following algebraic system,

$$\begin{bmatrix} \omega + q^2 & -v_p p_0 q^2 \\ -h_p & \omega + d q^2 - h_c \end{bmatrix} \begin{pmatrix} p_1 \\ c_1 \end{pmatrix} = \begin{pmatrix} 0 \\ 0 \end{pmatrix}. \quad (\text{S13})$$

To get a nontrivial/nonzero perturbation, the determinant of the matrix must be zero. Then,

$$(\omega + q^2)(\omega + d q^2 - h_c) - v_p p_0 q^2 h_p = 0. \quad (\text{S14})$$

Expanding,

$$\omega^2 + \underbrace{(q^2 + d q^2 - h_c)}_B \omega + \underbrace{q^2(q^2 d - h_c - v_p p_0 h_p)}_C = 0. \quad (\text{S15})$$

Solving for ω , we get $\omega = (-B \pm \sqrt{B^2 - 4C})/2$. Note that $B > 0$ since $h_c < 0$. Thus, to get instability with $\omega > 0$, we must have $C < 0$. This is not possible since both $h_c, h_p < 0$. Therefore, it is not possible to get spatial instability in this system regardless of the form $h(c, p)$.

2 Foragers and Exploiters Model

We now consider the model for foragers (with density $P(x, t)$), which move up food gradients. The second group consists of *exploiters*, with density $S(x, t)$, which move up gradients of forager density. The full unscaled system consists of

$$\frac{\partial P}{\partial t} = D_p \frac{\partial^2 P}{\partial x^2} - \chi_p \frac{\partial}{\partial x} \left(P \frac{\partial C}{\partial x} \right), \quad (\text{S16a})$$

$$\frac{\partial S}{\partial t} = D_p \frac{\partial^2 S}{\partial x^2} - \chi_s \frac{\partial}{\partial x} \left(S \frac{\partial P}{\partial x} \right), \quad (\text{S16b})$$

$$\frac{\partial C}{\partial t} = D_c \frac{\partial^2 C}{\partial x^2} - \Lambda(P + S)C - MC + R. \quad (\text{S16c})$$

Here, we assume that both types have the same random mobility coefficient D_p . The foragers are attracted by the gradient of food with the prey-taxis coefficient χ_p . Meanwhile the exploiters move up the gradient of foragers with a taxis coefficient χ_s . Preys are consumed at a rate Λ by both forager and exploiters. As before, we assume that the prey accumulates by migration or reproduction at rate R and decays at rate M . We impose no-flux boundary conditions at $x = 0$ and L , and obtain the following conservation equations for foragers and exploiters,

$$\int_0^L P(x, t) dx = \Phi_p \quad \text{and} \quad \int_0^L S(x, t) dx = \Phi_s \quad (\text{S17})$$

We denote the total population of foragers as $\Phi_{tot} = \Phi_p + \Phi_s$.

2.1 Nondimensionalization

As before, we performed non-dimensionalization using a similar scaling,

$$x = \hat{X}\bar{x} = L\bar{x}, \quad t = \hat{T}\bar{t} = \frac{L^2}{D_p}\bar{t}$$

$$P = \hat{P}\bar{p} = \frac{\Phi_{tot}}{L}\bar{p}, \quad S = \hat{S}\bar{s} = \frac{\Phi_{tot}}{L}\bar{s}, \quad C = \hat{C}\bar{c} = C_{max}\bar{c} = \max_{0 \leq x \leq L} C(x, 0)\bar{c}. \quad (\text{S18})$$

This results in the following system of non-dimensionalized equations,

$$\frac{\partial \bar{p}}{\partial \bar{t}} = \frac{\partial^2 \bar{p}}{\partial \bar{x}^2} - v_p \frac{\partial}{\partial \bar{x}} \left(\bar{p} \frac{\partial \bar{c}}{\partial \bar{x}} \right), \quad (\text{S19a})$$

$$\frac{\partial \bar{s}}{\partial \bar{t}} = \frac{\partial^2 \bar{s}}{\partial \bar{x}^2} - v_s \frac{\partial}{\partial \bar{x}} \left(\bar{s} \frac{\partial \bar{p}}{\partial \bar{x}} \right), \quad (\text{S19b})$$

$$\frac{\partial \bar{c}}{\partial \bar{t}} = d \frac{\partial^2 \bar{c}}{\partial \bar{x}^2} - \lambda(\bar{p} + \bar{s})\bar{c} - \mu\bar{c} + r. \quad (\text{S19c})$$

Henceforth, we drop the bar superscript from all the non-dimensionalized variables. The nondimensional parameters are defined as follows:

$$v_p = \frac{\chi_p \hat{C} \hat{T}}{L^2} = \frac{\chi_p C_{max}}{D_p}, \quad v_s = \frac{\chi_s \hat{P} \hat{T}}{L^2} = \frac{\chi_s}{D_p} \frac{\Phi_{tot}}{L}, \quad d = \frac{D_c}{D_p},$$

$$\lambda = \Lambda \hat{T} \hat{P} = \frac{\Lambda L \Phi_{tot}}{D_p}, \quad \mu = M \hat{T} = \frac{M L^2}{D_p}, \quad \text{and} \quad r = R \frac{\hat{T}}{\hat{C}} = \frac{R L^2}{D_p}. \quad (\text{S20})$$

The parameters have meanings analogous to those in the simpler model. Finally, following the above scaling, the conservation conditions (S17) become

$$\int_0^1 (p(x, t) + s(x, t)) dx = 1, \quad (\text{S21a})$$

$$\int_0^1 p(x, t) dx = \phi_p, \quad \int_0^1 s(x, t) dx = 1 - \phi_p. \quad (\text{S21b})$$

Now, ϕ_p represents the fraction of foragers in the population while $1 - \phi_p$ gives the fraction of exploiters.

3 Advantage of Strategies for Exploiters vs Foragers

To compare the benefit of being a forager vs. an exploiter, we define the average *instantaneous* per-capita rate of food consumption f_s, f_p by a typical individual in each group:

$$f_p(t) = \frac{\int_0^1 \lambda p(x, t) c(x, t) dx}{\int_0^1 p(x, t) dx} = \frac{\int_0^1 \lambda p(x, t) c(x, t) dx}{\phi_p}, \quad (\text{S22a})$$

$$f_s(t) = \frac{\int_0^1 \lambda s(x, t) c(x, t) dx}{\int_0^1 s(x, t) dx} = \frac{\int_0^1 \lambda p(x, t) c(x, t) dx}{1 - \phi_p}. \quad (\text{S22b})$$

The cumulative per capita food intake for each type, F_p and F_s , is obtained by integrating over time,

$$F_p(t) = \int_0^t f_p(s) ds \quad \text{and} \quad F_s(t) = \int_0^t f_s(s) dt. \quad (\text{S23})$$

We use the ratio of these two values as an indicator of the relative success of the two strategies. We define

$$b(t) = \frac{f_s(t)}{f_p(t)}, \quad B(t) = \frac{F_s(t)}{F_p(t)}, \quad (\text{S24})$$

so that $b(t)$ measures the instantaneous relative advantage over time while B measures the cumulative relative advantage (“benefit”) over time. Equally advantageous strategies imply $b = 1$ or $B = 1$. If exploiters are overall more successful in obtaining food then $b > 1, B > 1$.

3.1 Relative advantages with a static food patch

We start first by considering a static spatially nonuniform food patch $c(x)$ that does not get depleted and steady state forager/exploiter profiles $p(x), s(x)$. Having a static food distribution allows us to analytically obtain the steady state distributions of the foragers

and exploiters and calculate the benefit ratio (S24). We consider a patch of food with a single peak over the domain, of the form

$$c(x) = \cos(\pi x) + 1. \quad (\text{S25})$$

This trigonometric form allows us to analytically calculate the steady state distributions of foragers and exploiter with ease. Solving for the steady state solutions of (S19a)-(S19b) with the no flux boundary conditions, we obtain:

$$p(x) = p_0 \exp(v_p c(x)) \quad \text{and} \quad s(x) = s_0 \exp(v_s p(x)), \quad (\text{S26})$$

where the constant p_0 and s_0 are to be computed to obtain the corresponding fraction of foragers and exploiters, i.e.

$$\int_0^1 p(x) dx = \phi_p \Rightarrow p_0 = \frac{\phi_p}{\int_0^1 \exp(v_p c(x)) dx}, \quad (\text{S27})$$

$$\int_0^1 s(x) dx = 1 - \phi_p \Rightarrow s_0 = \frac{1 - \phi_p}{\int_0^1 \exp(v_s p(x)) dx}. \quad (\text{S28})$$

Thus, the steady state solutions have explicit dependence on ϕ_p , v_p and v_s . From (S24), we can also have

$$F_p = \frac{1}{\phi_p} \int_0^1 c(x) p(x) dx, \quad F_s = \frac{1}{1 - \phi_p} \int_0^1 c(x) s(x) dx, \quad B = \frac{F_s}{F_p}. \quad (\text{S29})$$

The integrals can be computed numerically, leading to B which depends on three parameters ϕ_p , v_p and v_s . In Figure 3 of the main paper, we show the neutral boundary curve for which $B = 1$ for three different values of the fraction of foragers, ϕ_p . Exploiters have the advantage above the curve, and foragers below the curve. For small v_p , the value of v_s for $B = 1$ is initially relatively constant (plateau). Here, the distribution of foragers is approximately uniform in space with $p(x) \sim \phi_p$ with very small gradient. In the limiting case of $v_p = 0$, we can compute the corresponding value of v_s for which $B = 1$ to be

$$v_s = \frac{\ln(1 - \phi_p)}{\phi_p}. \quad (\text{S30})$$

Hence, we see that for small v_p values, the corresponding value of v_s is relatively constant and is simply determined by the value of ϕ_p . This explains the plateau at small v_p . As v_p is increased, the equal benefit v_s value begins to drop. With increasing v_p value, foragers have greater prey taxis value, so the forager distribution becomes more peaked towards the maximum prey location and it has larger gradient. In this case, the value of the exploiter taxis parameter v_s need not be as large in order to still achieve $B = 1$.

3.2 Relative advantage with a nonrenewable resource.

Here we discuss relative advantages of the strategies when food is depleted by consumption. The full model is given in Eqs. (S19) but to model food being depleted, we assume its

production rate and its basal decay rate are zero, so $r = 0$ and $\mu = 0$ in (S19c), so that only consumption by foragers and exploiters is considered. We start with a normalized Gaussian (bell-shaped) initial resource distribution to model a fresh food patch, centered at $x = 0$, with characteristic “width” σ :

$$c(0, x) = \frac{1}{\sqrt{2\pi}\sigma} \exp\left(-\frac{x^2}{2\sigma^2}\right), \quad (\text{S31})$$

The normalization constant assures that each test simulation uses the same total amount of food, which is simply distributed more widely (large σ) or clumped (small σ). For the populations, we assumed an initial uniform density of each type, with proportions $p(0, x) = \phi_p$ and $s(0, x) = \phi_s = 1 - \phi_p$.

In Fig. S1, we considered the effect of varying the forager taxis parameter v_p for three values of v_s . As v_p is increased, the relative success of the exploiters decreases. On the other hand, when $v_s \gg v_p$ the exploiters effectively match the location of the foragers and the food exposure is the same for the two groups giving $B = 1$. For $v_p \gg v_s$ the ratio B reaches another limiting value below 1. In this limit, the exploiters find a little food simply due to their initial uniform distribution.

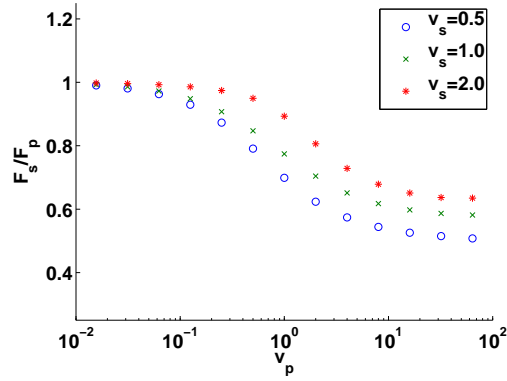


Figure S1: A plot that shows the effect of varying v_p for fixed values of v_s .

3.3 Model variants

The results described in the paper were based on a specific model. However, to check the robustness of our conclusions we carried out tests to see how slightly changing the model affects those conclusions. We looked at a number of variants, but here we present only two biologically relevant scenarios.

- *Effect of cost associated with primary foraging*

We modified the model by incorporating a cost to the primary foragers. (This could stem from energy expenditure for exposing or chasing prey.) In Figure S2, we redefine the relative success of exploiters to be $B = Fs/(F_p - C_p)$ where C_p depicts the constant cost to the foragers. In comparison to Fig. 4 in the main manuscript (where $C_p = 0$), here we see a wider parameter regime where $B > 1$, as expected.

- *Effects of exploiter sensing food directly*

Suppose that exploiters also search for resources on their own (though with lower sensing acuity than foragers). Then, the modified equation for S is

$$\frac{\partial s}{\partial t} = \nabla^2 s - v_s \nabla \cdot [s \nabla p] - \alpha v_p \nabla \cdot [s \nabla c], \quad (\text{S32})$$

The plot of relative success as the parameter α is varied is shown in Figure S3. In this case, we see an increase in the relative success of the exploiters. The success increases when α increases, and eventually, exploiters have a greater advantage than foragers.

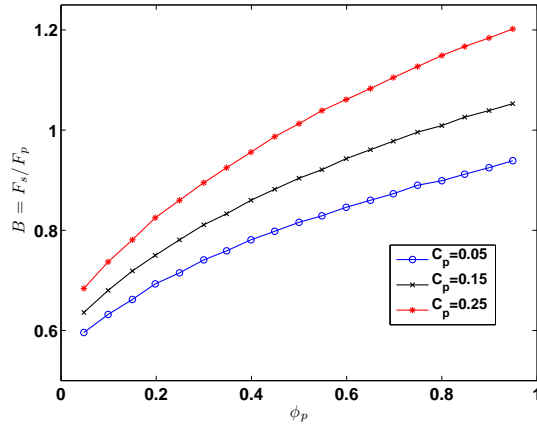


Figure S2: As in Fig. 4 with patch width $\sigma = 0.1$ but with foraging cost C_p so that the relative success is $F_s/(F_p - C_p)$.

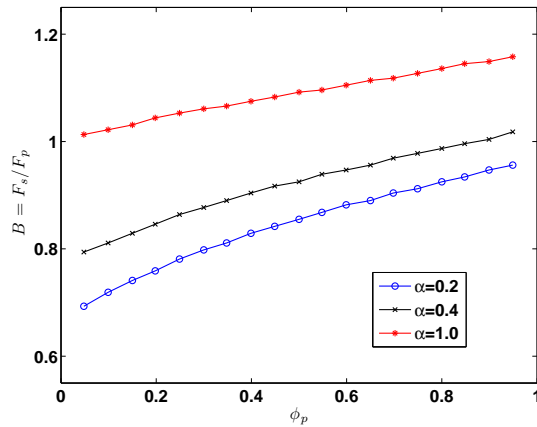


Figure S3: As in Fig. 4 but with the exploiters also detecting the prey directly with taxis parameter αv_p (where $\alpha \leq 1$).

4 Linear Stability Analysis for Foragers-Exploiters Model

Here we perform the linear stability analysis of the full forager-exploiter-prey (PSC) system as given in Eqn. (S19). The reader may wish to consult [1] for analysis of a related (but more general) case of two interacting populations with one common attractor.

The homogenous steady state solution (HSS) for this system is

$$p(x, t) = \phi_p, \quad s(x, t) = 1 - \phi_p, \quad c(x, t) = c_o = \frac{r}{\mu + \lambda}. \quad (\text{S33})$$

To study the stability of this uniform steady state, we determine whether small perturbations will grow in time. Let

$$p(x, t) = \phi_p + \tilde{p}(x, t), \quad s(x, t) = (1 - \phi_p) + \tilde{s}(x, t), \quad \text{and} \quad c(x, t) = c_o + \tilde{c}(x, t) \quad (\text{S34})$$

where quantities with tildes are small. For this to be a solution, \tilde{p} , \tilde{s} , \tilde{c} need to satisfy the no flux boundary condition. Further, these must satisfy the conservation condition (S21), we assume

$$\int_0^1 \tilde{p}(x, t) dx = 0 \quad \text{and} \quad \int_0^1 \tilde{s}(x, t) dx = 0. \quad (\text{S35})$$

Substituting (S34) into the PDEs (S19) and keeping only terms up to first order, we get

$$\tilde{p}_t = \tilde{p}_{xx} - v_p \phi_p \tilde{c}_{xx}, \quad (\text{S36})$$

$$\tilde{s}_t = \tilde{s}_{xx} - v_s (1 - \phi_p) \tilde{p}_{xx}, \quad (\text{S37})$$

$$\tilde{c}_t = d\tilde{c}_{xx} - \lambda c_o (\tilde{s} + \tilde{p}) - (\lambda + \mu)\tilde{c}. \quad (\text{S38})$$

For ease of notation, from now on we denote $V_p = v_p \phi_p$, and $V_s = v_s (1 - \phi_p)$. We seek solutions for \tilde{p} , \tilde{s} , \tilde{c} of the form:

$$\tilde{p} = p_1 \cos(qx) \exp(wt), \quad \tilde{s} = s_1 \cos(qx) \exp(wt), \quad \tilde{c} = c_1 \cos(qx) \exp(wt). \quad (\text{S39})$$

To satisfy the no-flux and zero integral conditions, we need $q = n\pi$ where n is a non-zero integer. Substituting, we obtain the following algebraic equations:

$$p_1 w = q^2 (-p_1 + V_p c_1), \quad (\text{S40})$$

$$s_1 w = q^2 (-s_1 + V_s p_1), \quad (\text{S41})$$

$$c_1 w = -d c_1 q^2 - \lambda c_o (p_1 + s_1) - (\lambda + \mu) c_1, \quad (\text{S42})$$

or in the matrix-vector form,

$$\begin{bmatrix} w + q^2 & 0 & -V_p q^2 \\ -V_s q^2 & w + q^2 & 0 \\ \lambda c_o & \lambda c_o & w + d q^2 + (\lambda + \mu) \end{bmatrix} \begin{pmatrix} p_1 \\ s_1 \\ c_1 \end{pmatrix} = \begin{pmatrix} 0 \\ 0 \\ 0 \end{pmatrix}. \quad (\text{S43})$$

To obtain p_1 , s_1 , and c_1 not all zero, the determinant of the matrix must be zero. This results in the following cubic equation for the eigenvalue w ,

$$w^3 + Aw^2 + Bw + C = 0, \quad (\text{S44})$$

where

$$A = (2 + d)q^2 + (\mu + \lambda), \quad (\text{S45})$$

$$B = (1 + 2d)q^4 + (\lambda c_o V_p + 2(\mu + \lambda))q^2, \quad (\text{S46})$$

$$C = dq^6 + (\lambda c_o V_p (1 + V_s) + (\mu + \lambda))q^4. \quad (\text{S47})$$

Using Descartes' rule of sign for polynomials, we first note that the number of positive real roots is always zero since $A, B, C > 0$ given any set of non-trivial parameter values. In fact, there are only two possibilities: (i) (S44) has three negative real roots, or (ii) it has one negative real root and a pair of complex-conjugate roots. Thus, we can conclude that any instabilities to the stationary solution must arise from the second case, namely when the complex-conjugate root transition from having a negative to a positive real part (Hopf bifurcation). Thus, no static standing pattern can arise in this system and only oscillatory patterns can be found.

We continue the analysis by using the Routh-Hurwitz condition to determine when the complex root pair has positive real part. It can be shown that this occurs when $AB - C < 0$. We write this condition as a function of the wave number q . For instability, we need

$$F(q^2) = AB - C = q^2(\alpha q^4 + \beta q^2 + \eta) < 0, \quad (\text{S48})$$

where the coefficients are

$$\alpha = 2(d + 1)^2, \quad (\text{S49})$$

$$\beta = 4(\lambda + \mu)(d + 1) + V_p \lambda c_o (1 + d - V_s), \quad (\text{S50})$$

$$\eta = (\lambda + \mu)[V_p \lambda c_o + 2(\lambda + \mu)]. \quad (\text{S51})$$

Note that $\alpha, \eta > 0$ while β could have either sign depending on V_s . To find instability, we now seek modes $F(q^2) < 0$. As illustrated in Figure S4, there are three distinct possibilities, classified by the number of real positive roots of F :

- (A) No positive root: If $\beta \geq 0$ then the roots of the quadratic equation $\alpha x^2 + \beta x + \eta = 0$ are either real with negative signs, or complex. Similarly, if $\beta < 0$ but $\beta^2 - 4\alpha\eta < 0$, then the roots of $\alpha x^2 + \beta x + \eta = 0$ are complex, so $F(q^2) \geq 0$ for all q . Thus, no instability will arise in this case.
- (B) One positive roots: If $\beta < 0$ and $\beta^2 - 4\alpha\eta = 0$, then $q^2 = 0$ and $q^2 = -\beta/2\alpha$ are both roots but $F(q^2) \geq 0$ still. This case will also not yield any unstable solution.
- (C) Two positive roots: If $\beta < 0$ and $\beta^2 - 4\alpha\eta > 0$, then there are two positive roots to $\alpha x^2 + \beta x + \eta = 0$ and there is a range of q where $F(q^2) < 0$, consistent with instability. We examine this case further.

For the instability case (C), the relationship between the root condition above and the parameter values used in the model (see definitions of α, β , and η in (S49)-(S51)) can be analyzed further:

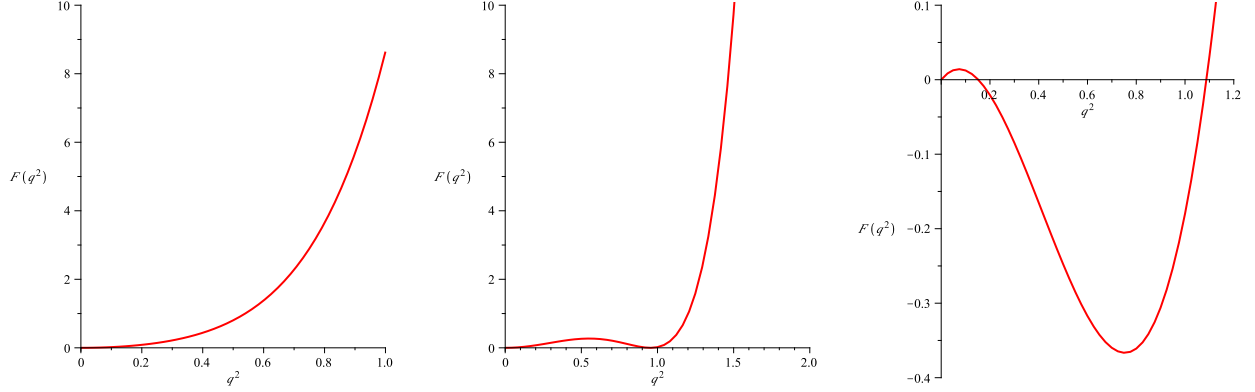


Figure S4: Sketch of different possible behavior for $F(q^2)$, from left to right, case (A), (B), and (C), where $F(q^2)$ has one, two, or three positive roots respectively.

(I) First, to have $\beta < 0$, we need

$$(1+d) \left(4 \frac{\lambda + \mu}{V_p \lambda c_o} + 1 \right) < V_s. \quad (\text{S52})$$

(II) Next, by manipulating the algebraic expressions for $\beta^2 - 4\alpha\eta > 0$, we obtain the inequality,

$$8(d+1) \frac{\lambda + \mu}{V_p \lambda c_o} < \frac{(V_s - (d+1))^2}{V_s}. \quad (\text{S53})$$

In essence, both conditions can be interpreted in terms of a threshold value for V_s for the existence of a range of wave numbers q that produce instability ($F(q^2) < 0$). (See Fig. S4, right panel.) The two inequalities (S52)-(S53) can be simplified further into one (equation S58). Readers can skip the next paragraph if they are not interested in the details of the algebraic manipulations.

Let $\xi = \frac{V_p \lambda c_o}{\mu + \lambda}$. Then the two inequality can be rearranged as follows:

(I) Inequality (S52) becomes

$$\frac{(4 + \xi)(d+1)}{\xi} < V_s. \quad (\text{S54})$$

(II) Inequality (S53) can be rearranged to

$$\frac{8}{\xi} < \frac{(V_s - (d+1))^2}{V_s(d+1)} \equiv H(V_s). \quad (\text{S55})$$

In Figure S5, a plot of the function $H(V_s)$ is seen to cross the line $y = 8/\xi$ at two places, namely

$$V_s^+ = \frac{(\xi + 4)(d+1) + 2(d+1)\sqrt{2(\xi + 2)}}{\xi}, \quad V_s^- = \frac{(\xi + 4)(d+1) - 2(d+1)\sqrt{2(\xi + 2)}}{\xi} \quad (\text{S56})$$

To satisfy the inequality (S53), we need $V_s < V_s^-$ or $V_s > V_s^+$.

However, we see that if $V_s < V_s^-$, then the first inequality will not be satisfied. However, if $V_s > V_s^+$, the first inequality is immediately satisfied. Thus it is only possible to obtain instability if

$$\frac{(\xi + 4)(d + 1) + 2(d + 1)\sqrt{2(\xi + 2)}}{\xi} < V_s, \quad (\text{S57})$$

or substituting, $\xi = \frac{V_p \lambda c_o}{\mu + \lambda}$ back,

$$(d + 1) \left(1 + \frac{4(\mu + \lambda)}{V_p \lambda c_o} + \frac{2\sqrt{\mu + \lambda}}{V_p \lambda c_o} \sqrt{2(V_p \lambda c_o + 2(\mu + \lambda))} \right) < V_s. \quad (\text{S58})$$

The inequality (S58) is shown graphically in Figure S5 as $V_s > V_s^+$.

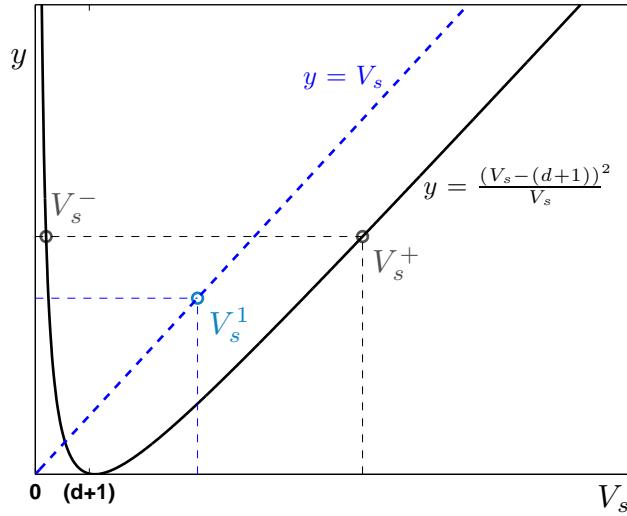


Figure S5: Threshold condition for V_s : the critical value, V_s^* , is given by the maximum of V_s^1 (due to (S52)) and V_s^+ (from (S53)). When $V_s > V_s^*$, the linear stability analysis predicts that there is a certain range of q such that $F(q^2) < 0$, giving rise to instability of the homogenous steady state and formation of the dynamic pattern.

A simplified inequality can be found by observing that when V_s is large enough, the curve $y = \frac{(V_s - (d + 1))^2}{V_s}$ can be approximated by the line $y = V_s - 2(d + 1)$. Thus, applying inequality (S53), we have

$$\frac{8(\lambda + \mu)(d + 1)}{V_p \lambda c_o} + 2(d + 1) \lesssim V_s. \quad (\text{S59})$$

Recalling that $V_p = v_p \phi_p$ and $V_s = v_s(1 - \phi_p)$, and since $c_o = r/(\lambda + \mu)$,

$$\frac{8(\lambda + \mu)^2(d + 1)}{v_p \phi_p \lambda r} + 2(d + 1) \lesssim v_s(1 - \phi_p). \quad (\text{S60})$$

This leads to Eqn. [3] in the main article, arriving at the condition for instability.

5 Switching between the strategies

Here we investigate how switching between strategies affects the dynamics and population structure. In this section we describe only behavioural switching that occurs on a short timescale relative to the life span of individuals, e.g. by learning or copying behaviour of group-mates. To model behavioural switching, we set $h_p(p, s) \neq 0, h_s(p, s) \neq 0$ in Eqs. [2] and simulating the full model as described previously.

We considered a number of simple rules for switching

5.1 Random switching

The simplest mathematical case, random switching at some constant rate is included here. This case already reveals spatiotemporal dynamics that are seen in more realistic model variants shown later. Here, we set $h_p(p, s) = as - bp = -h_s(p, s)$ in Eqs. [2]. For low values of the switching parameters a, b , results are very similar to those previously discussed. In Fig. S6, we set $a = b = k$ (equal switching from each strategy) and varied the switching rate k (as well as v_s and v_p). Our numerical exploration suggests that the switching terms have a destabilizing effect. For the basic case shown in Fig. 2 ($v_s = v_p = 10$), we see that increasing the switching rate leads to dominance of a higher mode of oscillation. Starting with a case where no pattern forms and there is no switching ($k = 0$), we find that increasing k leads to the emergence of an oscillatory pattern and in a high switching rate regime, we find a previously absent standing wave pattern. This pattern arises from damped cycles which stall with p and s high at one end of the domain, and resource peaks high at the opposite end. This counterintuitive segregation stems from the fact that extremely rapid switching between strategies results in conflicting cues for the preferred direction of motion (towards food vs towards other foragers). This can lead to a self-reinforced peak of foragers in the “wrong place”, that overexploit local resources even though better patches are available. This type of stagnation is seen only in a range of parameters that are at the limit of rapid switching. This case, though mathematically interesting is less relevant biologically.

We also looked at the fraction of foragers and exploiters over time (as in Fig. 6). For the constant switching case, the long term fraction of each type is constant over time. This stems from the fact that the switching is spatially independent and there is a tendency to equilibrate at the ratio $s/p = b/a$ locally, as well as globally (integrated over the domain).

5.2 Switching based on perceived relative advantage

We next considered the biologically motivated case where switching stems from the perceived relative advantages of the strategies. We adopted the switching rates

$$s \rightarrow p : \alpha(b_i) = \frac{k}{(1 + b_i)}, \quad p \rightarrow s : \beta(b_i) = \frac{kb_i}{(1 + b_i)}, \quad (\text{S61})$$

with k a maximal switching rate and b_i a measure of the perceived benefit to scrounging. We considered three possible measures for the perceived scrounging benefit b_i . Note in this scheme, when $b_i > 1$, then $\beta > \alpha$. Thus as the benefit to exploiters increases, the switching rate to adopt this strategy also increases. The reverse is true when $b_i < 1$. When $b_i = 1$,

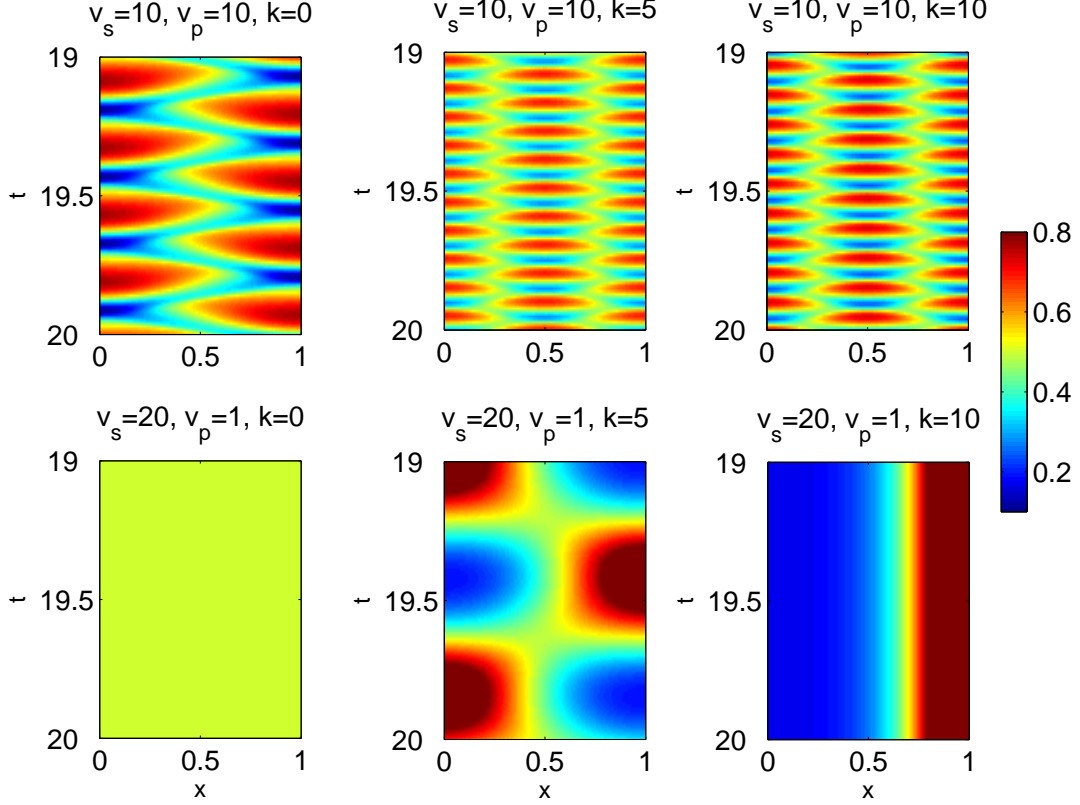


Figure S6: Spatiotemporal profile for exploiter density $s(x, t)$ with constant switching term $h_p(p, s) = -h_s(p, s) = as - bp$. Here we set switching rates equal $a = b = k$. *Top panels:* $v_s = v_p = 10$, and switching rate increasing from left to right, i.e. $k = 0, 5, 10$ (no switching, intermediate, and rapid switching) *Bottom panels:* as above, but with $v_s = 20$ and $v_p = 1$: The uniform steady state solution is stable with no switching ($k = 0$), and standing wave pattern is observed for high switching rate ($k = 10$). All other parameter values as in Fig. 2.

both strategies yield the same advantage and $\beta = \alpha = k/2$, so there is an equal likelihood to switch from one strategy to another.

5.2.1 Purely local sensing

We first considered purely local sensing of information, where an individual at position x and time t decides to switch based only on food and densities of foragers and exploiters at (x, t) . This is a limiting case of short-range sensing when the sensing range is very small relative to patch and domain sizes. For this case, we used

$$f_{p,loc}(x, t) = \frac{\lambda p(x, t)c(x, t)}{\int_0^1 p(y, t)dy} = \frac{\lambda p(x, t)c(x, t)}{\phi_p(t)}, \quad (\text{S62})$$

$$f_{s,loc}(x, t) = \frac{\lambda s(x, t)c(x, t)}{\int_0^1 s(y, t)dy} = \frac{\lambda s(x, t)c(x, t)}{\phi_s(t)}, \quad (\text{S63})$$

for which

$$b_{local}(x, t) = \frac{f_{s,loc}(x, t)}{f_{p,loc}(x, t)} = \frac{s(x, t) \phi_p(t)}{p(x, t) \phi_s(t)}$$

Then, it is evident that the switching at different locations in the domain, $b_{local}(x, t)$ depends only on the ratios of scroungers to producers locally (at x) and globally (averaged over the domain), but not at all on the local food density (so long as $c(x, t) > 0$)

In this extreme local limit, the switching behavior yields no new spatiotemporal dynamics. In simulations over a wide range of parameter values (same values as we used in Fig. S6), we saw only behavior that was already captured by the simplest model without switching. This is not too surprising, in view of the fact that purely localized switching does not bias decisions based on food availability, as shown in the expression for $b_{local}(x, t)$. The same conclusion can be drawn for switching with a very small (but not purely local) sensing range r_{sense} , where an integral of the form $\int p(x, t)c(x, t)dx$ is well approximated by the expression $p(x, t)c(x, t)r_{sense}$.

5.2.2 Long range (global) sensing

This is a second limiting case, when the sensing range is very large relative to typical domain size. Here switching is assumed to depend on per capita food consumption average over distances comparable to the entire domain. Hence, we defined

$$b_{global}(t) = \frac{f_s(t)}{f_p(t)},$$

where f_s, f_p are given by Eqs. S22, i.e., each is a per-capita food consumption averaged over the entire domain $0 \leq x \leq 1$.

Results are similar to those shown of Fig. S6. However, the fractions of foragers and exploiters can vary in time as shown in Fig. 6 of the main paper. Here, the switching rate is found to vary in space and time, depending on the relative advantage for exploiters.

For completeness, in Fig. S7, we show spatiotemporal dynamics of all three variables when $v_s = 20$ and $v_p = 1$ (i.e. when the uniform steady-state is stable without switching).

5.2.3 Finite sensing range

Here we considered the case that individuals have some finite sensing range of radius R and that they base switching decisions on perceived relative per-capita food consumption of the strategies within this finite sensing range. Then

$$f_{p,R}(x, t) = \frac{\int_{x-R}^{x+R} \lambda p(y, t)c(y, t)dy}{\int_0^1 p(y, t)dy} = \frac{\int_{x-R}^{x+R} \lambda p(y, t)c(y, t)dy}{\phi_p(t)}, \quad (\text{S64})$$

$$f_{s,R}(x, t) = \frac{\int_{x-R}^{x+R} \lambda s(y, t)c(y, t)dy}{\int_0^1 s(y, t)dy} = \frac{\int_{x-R}^{x+R} \lambda p(y, t)c(y, t)dy}{\phi_s(t)}, \quad (\text{S65})$$

and we take

$$b_R(t) = \frac{f_{s,R}(t)}{f_{p,R}(t)},$$

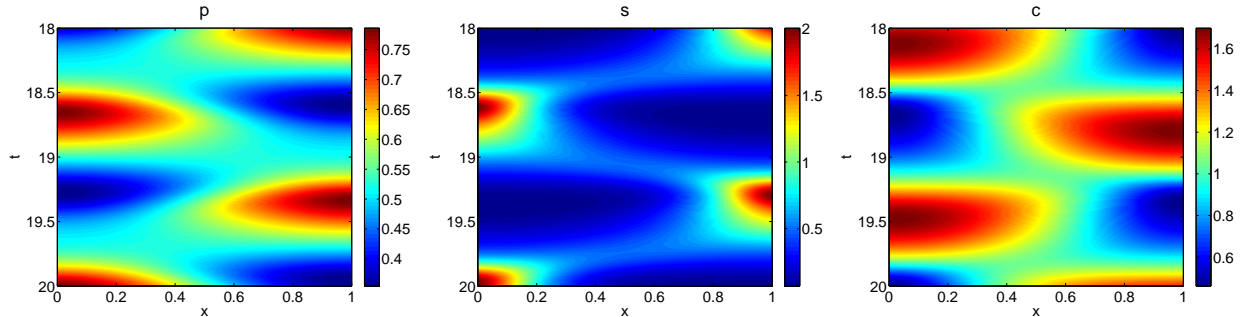


Figure S7: Oscillatory spatial patterns in forager, exploiter, and resource densities obtained when switching is based on relative per capita food consumption averaged over the entire domain, b_{global} . Solution corresponds to the bottom panel of Figure 6 of the main manuscript and uses the same parameter values ($v_s = 20$, $v_p = 1$, and $k = 19$; note that $k = 20$ yields a standing pattern).

to determine the switching rate.

As we increase the sensing range, R , we observe a transition between the two previously described limiting cases. Using $v_s = 20$ and $v_p = 1$, we found that the uniform steady-state solution is stable until $R \approx 0.4$. In Fig. S8, we showed two spatiotemporal oscillatory patterns obtained as R is increased. The fraction of foragers and exploiters also oscillates in time as shown in Fig. S9 with increasing amplitude as the sensing range, R , is increased.

6 Reproductive fitness depends on relative advantage of strategies

Reproduction usually takes place on a slower time scale than movement and food consumption. Hence, we avoid simply adding growth rates to the taxis PDEs. Instead, we subdivided the problem into dynamics within and between (non-overlapping) generations.

Briefly, we assumed that the model (S19) describes the short-term interactions and resource consumption of the population during a single generation, for time $t_0 \leq t \leq t_{gen}$, where t_{gen} is the length of a generation. At $t = t_{gen}$, we assumed that all individuals produce progeny, based on the per capita share of the resource that they consumed (averaged over the entire time $t_0 \leq t \leq t_{gen}$). Parents die, and are replaced by the next generation (semelparous reproduction). We then assumed that the ratio of the two types of progeny reflects the relative advantage of the two strategies.

This basic idea can be implemented in many ways, taking a variety of reproductive rules (Malthusian, logistic, competitive, etc.). Most such assumptions lead to net growth in the total size of the population, and (since growth described by exponentials or other nonlinear functions) the ratio of foragers to exploiters is not easily expressed in closed form. Consequently, the system has to be explored numerically, leading to combinatorial explosion in the number of possible assumptions, parameter values, and conditions to test.

Such studies form interesting future directions, but here we chose an alternative that

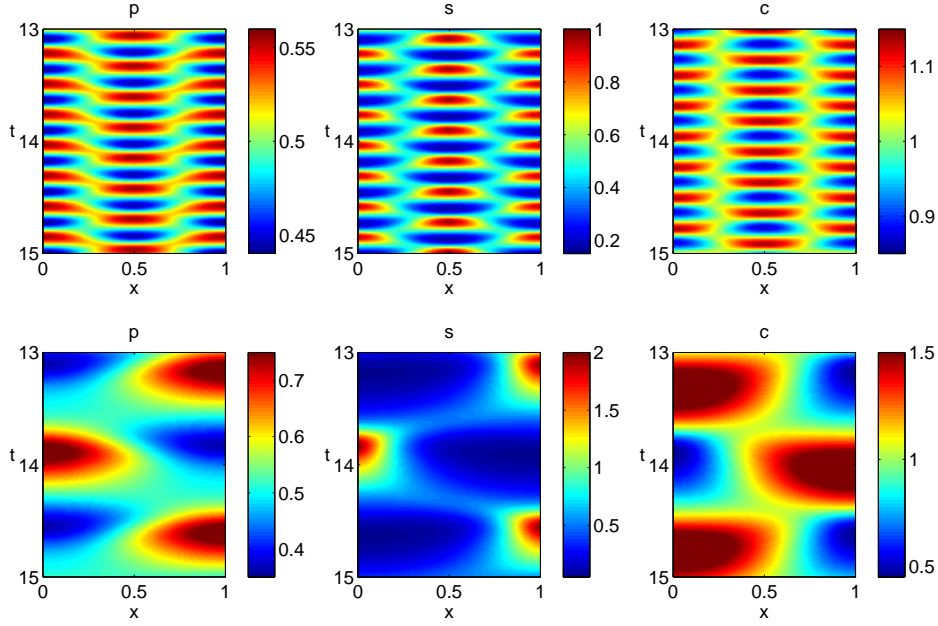


Figure S8: Oscillatory spatial patterns in forager, exploiter, and resource densities obtained when switching is based on perceived relative advantage $b_R(t)$ over some finite sensing range R ($v_s = 20$, $v_p = 1$, $k = 20$, *top*: $R = 0.4$ and *bottom*: $R = 0.8$).

leads to a simple, yet elegant way of linking one generation to the next. We used the rule

$$s(T + 1) = \alpha \frac{F_s(T)}{F(T)}, \quad p(T + 1) = \alpha \frac{F_p(T)}{F(T)}, \quad (\text{S66})$$

for T the generation number, and $F = F_s + F_p$. This rule could describe a competition for some fixed number of “nesting sites”, with relative success determined by the energy

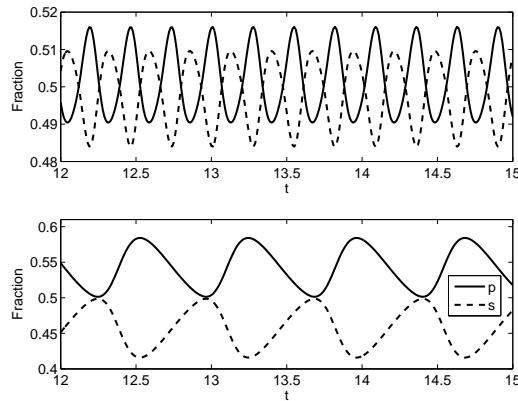


Figure S9: Dynamics of the fraction of foragers and exploiters. Parameter values as in Fig. S8 ($v_s = 20$, $v_p = 1$, $k = 20$, *top*: $R = 0.4$ and *bottom*: $R = 0.8$).

acquired during the timespan $0 < t < t_{gen}$. Then (S66) implies that

$$s(T + 1) + p(T + 1) = \alpha = \text{constant},$$

so the total population is constant, and we can divide each of (S66) by α and rearrange terms to obtain

$$\phi_p(T + 1) = \frac{F_p(T)}{F(T)} = \frac{F_p(T)}{F_p(T) + F_s(T)} = \frac{1}{1 + F_s(T)} = \frac{1}{1 + B(T)}, \quad (\text{S67})$$

The simplicity of this rule allows us to use results at hand to understand long-term dynamics as a proof of principle.

As discussed in the main paper, $B(T)$ can be expressed as some relationship between the (fixed) proportion $\phi_p(T)$ of foragers within the given generation, and other parameters that characterize the foragers and food distribution. The latter gives rise to some relationship, of the form

$$B(T) = \frac{F_s(T)}{F_p(T)} = f(\phi_p(T), \sigma), \quad (\text{S68})$$

where σ is a vector of parameters. As an example, we have curves in Fig. 4 of the main paper with σ representing characteristic food patch width. (This is a specific example, but other assumptions about the food and other parameter values for the strategies would produce particular curves of related shape.) As a general rule, we expect $f(\phi_p(T), \sigma)$ to be an increasing function of ϕ_p , since, as argued in the paper, an exploiter does better (resulting in larger value of B) when the population has more foragers to follow. Thus the derivative $df/d\phi_p$ is positive.

We can use both Eqs. (S67) and (S68) to write the following discrete difference equation linking successive generations:

$$\phi_p(T + 1) = g(\phi_p, \sigma) = \frac{1}{(1 + f(\phi_p(T), \sigma))}. \quad (\text{S69})$$

Analysis of such equations is easily accomplished. First note that steady states satisfy

$$\phi_{p,SS} = \frac{1}{(1 + f(\phi_{p,SS}, \sigma))}. \quad (\text{S70})$$

These are located at the intersection of the two curves represented by equations Eqs. (S67) and (S68). Moreover the stability of the steady state is conditional on $|dg/d\phi_p| < 1$ (with the derivative evaluated at the steady state). But

$$\left. \frac{dg}{d\phi_p} \right|_{SS} = - \frac{1}{(1 + f(\phi_{p,SS}, \sigma))^2} \frac{df}{d\phi_p}.$$

By previous remarks, this expression is always negative, signifying that decay to steady state (if stable) is always accompanied by damped oscillations, as shown in Fig. 7 of the main paper. The first term is always smaller than 1 in magnitude. Thus stability hinges on the magnitude of $df/d\phi_p$ at the steady state. In Fig. 7 of the main paper, $|df/d\phi_p| < 1$ (the curve was sufficiently shallow at the crossover point) so that the steady state is stable. Here

we consider the possibility that other instances (values of parameters, food distributions, or interactions) could, in principle, lead to a steeper curve. This can lead to instability of the steady state so that the population structure would fluctuate between low and high proportions of foragers in successive generations.

We can capture the inter-generational dynamics either by iterating the map in (S69), or, as shown in the paper, by bouncing between the curves $\phi_p(T), B(T), \phi_p(T + 1), B(T + 1) \dots$. While it is not our purpose here to systematically explore all possible shapes of the relationship $f(\phi_p, \sigma)$, we show in Fig S10 an illustrative schematic example where f is sufficiently steep that stable cycles are produced.

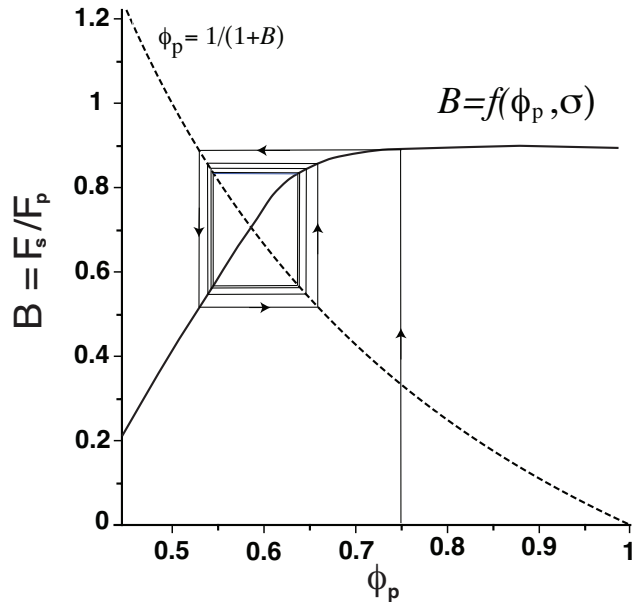


Figure S10: When the relationship between the fraction of foragers and the advantage to exploiters, $B(T) = f(\phi_p, \sigma)$, is sufficiently steep (which depends on a combination of parameters for interactions, domain, and food distribution), then it is possible in principle to obtain sustained fluctuations in the population structure over many generations. Low and high fractions of foragers will be seen in alternating generations in such cases.

7 Numerical Methods

Our numerical methods included a standard finite difference scheme for the diffusion terms, and a centered difference scheme for the nonlinear advection terms, resulting in a conservative scheme. Typical grid spacing for simulations were of size 0.005 (200 grid points), although finer grid solutions were computed in order to check for convergence. Time integration was handled explicitly, with the size of the time step being dictated by the size of the spatial discretization as well as model parameters such as v_s and v_p . Typical values were of size 10^{-5} . The zero-flux boundary condition was enforced by including ghost points outside the domain and relating the value of the solution at these points to values of the solution

at grid points inside the computational domain. All integrals of the solution (such as the computation of food contact) were computed using a midpoint approximation centered on the finite difference grid.

References

- [1] HORSTMANN D (2011) Generalizing the Keller-Segel Model: Lyapunov Functionals, Steady State Analysis, and Blow-Up Results for Multi-species Chemotaxis Models in the Presence of Attraction and Repulsion Between Competitive Interacting Species. *J Nonlinear Sci* 21: 231-270.